

QUASI-STEADY AERODYNAMIC AND MBD COUPLED FLIGHT SIMULATION OF FOLDING MORPHING UAV

Yikai Bu[1,2], Lei Qiao[*,1,2], Li Li[3], Haojie Feng[1,2] & Junqiang Bai[1,2]

[1]Unmanned System Research Institute, Northwestern Polytechnical University, Xi'an 710072, China
[2]National Key Laboratory of Unmanned Aerial Vehicle Technology, Xi'an 710072, China
[3]School of Future Transportation, Chang'an University, Xi'an, 710018, China
[*]Corresponding author: ql@nwpu.edu.cn

Abstract

Folding morphing aircraft exhibit strong aerodynamic–multibody coupling during airborne deployment due to large relative motions and flow disturbances. To address limitations in full-sequence deployment simulation and mechanism analysis, an aerodynamic–multibody coupled framework based on Kanes equations and a quasi-steady aerodynamic model is developed, where the multibody system is modeled as joint-constrained rigid bodies and aerodynamic loads are obtained by solving the inviscid Euler equations on Cartesian grids with bidirectional iterative coupling. Numerical simulations of an LG2K-like UAV at 4° angle of attack and 4° sideslip angle show pronounced asymmetric wing deployment for $\omega_y = \pm 1$ rad/s. For $\omega_y = 1$ rad/s, the maximum deployment difference reaches about 35° with full roll motion and slight center-of-mass motion, while for $\omega_y = -1$ rad/s the difference reduces to about 15° with a final roll angle of about 70° and smoother attitude evolution. In both cases, strong unsteady aerodynamic fluctuations are observed, indicating that the initial pitch rate significantly affects deployment synchronization, attitude response, and overall deployment stability and safety.

Keywords: folding morphing UAV, airborne deployment simulation, quasi-steady aerodynamic model, multibody dynamics

1. Introduction

Folding morphing UAVs exhibit strong aerodynamic–dynamic coupling during configuration transformation. Conventional design relies on repeated flight tests for performance evaluation, which are costly, time-consuming, and risky, and thus difficult to meet rapid development requirements [1]. To address this, the Arnold Engineering Development Complex (AEDC) proposed the concept of Virtual Flight Test (VFT) to reproduce flight processes using ground-based experiments [2, 3]. Early work mainly constructed aerodynamic databases from static force measurements [4, 5], while later studies introduced dynamic wind tunnel testing to capture motion-dependent aerodynamic effects [6, 7]. However, due to scaling effects, support interference, and cost constraints, wind tunnel data still deviate from real flight conditions and typically require correction [8, 9].

With the advancement of computational capability, numerical virtual flight methods have become a key focus in morphing aircraft research [10]. Extensive studies have addressed aerodynamic and dynamic modeling of morphing vehicles. Yue [11, 12] derived decoupled longitudinal dynamics for a Z-shaped folding-wing aircraft under a quasi-steady aerodynamic assumption. Tong [13, 14] developed a multibody dynamic model for an asymmetric variable-sweep UAV using Kanes method, capturing transient morphing behaviors. Shi et al. [15] constructed a large-scale morphing aircraft model using DATCOM-based aerodynamic derivatives to analyze stability. An [16] proposed an unsteady vortex lattice method to obtain aerodynamic and dynamic characteristics during wing sweep.

However, despite progress in aerodynamic modeling, multibody dynamics, and coupling strategies, a unified and efficient framework for simulating the full airborne deployment and deployment process of folding morphing UAVs is still lacking.

A coupled simulation framework based on Kanes equations and a quasi-steady Euler aerodynamic model is developed to simulate the full airborne deployment process of a folding morphing UAV from release to configuration unfolding. The method adopts joint-constrained rigid-body representations and computes aerodynamic loads by solving the inviscid Euler equations on Cartesian grids, with a time-marching strategy used for aerodynamic–dynamic coupling. A representative LG2K-like configuration is selected as the research object [17]. Numerical simulations under carrier wake conditions are performed to investigate asymmetric wing deployment and the resulting attitude response, providing a reference for dynamic analysis and attitude control design of folding morphing UAVs.

2. Modeling Method and Attitude Analysis

2.1 Quasi-Steady Aerodynamic Model and Coupling Method

A quasi-steady aerodynamicmultibody coupling method is developed to simulate the coupled aerodynamic loads and multibody dynamic response during the airborne deployment of a folding morphing UAV, with the flow field governed by the inviscid Euler equations in conservative form:

$$\frac{\partial \mathbf{U}}{\partial t}+\frac{\partial \mathbf{F}}{\partial x}+\frac{\partial \mathbf{G}}{\partial y}+\frac{\partial \mathbf{H}}{\partial z}=0 \tag{1}$$

The governing equations are discretized using a central-difference scheme with Jameson–Schmidt–Turkel (JST) artificial dissipation. A Cartesian structured grid is adopted.

A time-marching bidirectional coupling strategy is employed. At each time step, aerodynamic loads are computed from the current configuration and transferred to the multibody dynamics module to update velocities, angular velocities, and rigid-body attitudes under joint constraints. The updated configuration is then used for the next aerodynamic computation, forming an iterative coupling process.

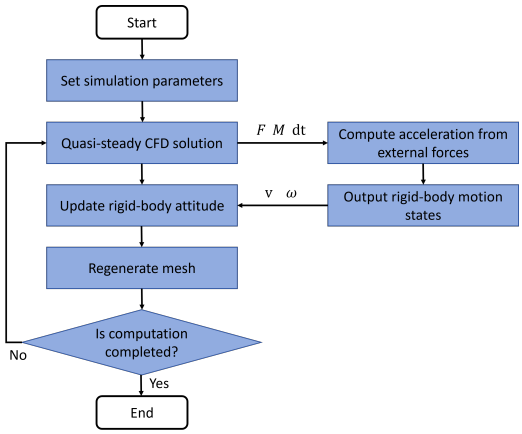


Figure 1 – Quasi-steady aerodynamic–multibody coupling framework

2.2 Multibody Dynamic Modeling Based on Kanes Equations

In the coupled framework described above, the multibody dynamics are formulated based on Kanes equations. As shown in Fig. 2, the vehicle is modeled as a tree-topology multibody system composed of rigid bodies connected by joints, with local coordinate systems defined on each body to describe relative motion.

Based on recursive kinematics, the system equations of motion are assembled using Kanes method by combining generalized inertia forces and external loads, including aerodynamic loads and gravity. The resulting governing equations can be written as

$$\sum_i \left(V_i^T m_i V_i + W_i^T I_i W_i\right)\cdot \ddot{q} = \sum_i \left[\left(F_i^T - \left(m_i \dot{V}_i \cdot \dot{q}_i\right)^T\right) V_i + \left(M_i^T - \left({}_0\omega_{0,i} \times \left(I_i \cdot {}_0\omega_{0,i}\right) + I_i \cdot \dot{W}_i \cdot \dot{q}\right)^T\right) W_i\right] \tag{2}$$

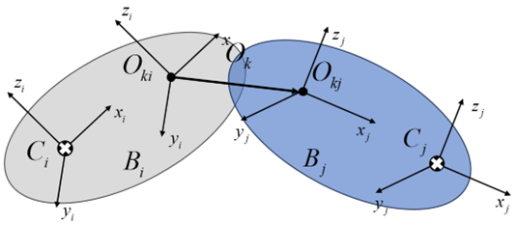


Figure 2 – Adjacent rigid bodies and the coordinate systems established on them

2.3 Dynamic Model of LG2K-Type Folding Morphing UAV

An LG2K-type folding morphing UAV is selected for simulation to support attitude analysis and numerical validation. A body-fixed coordinate system is defined with the X-axis pointing forward, the Y-axis to the right wing, and the Z-axis downward. A symmetric deployment mechanism is adopted, avoiding inherent geometric asymmetry in aerodynamic moments. The fuselage length is approximately 3.9 m and the wingspan is 7–8 m, as shown in Fig. 3.

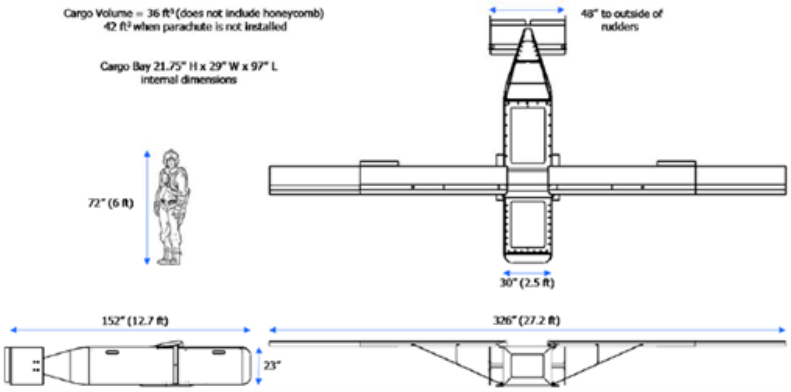
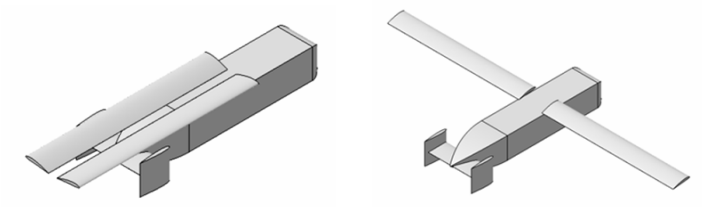


Figure 3 – Three-view drawing of the LG2K folding morphing UAV[17]

The geometric model is simplified from the LG2K prototype by neglecting detailed structural components. A LG2K-type folding morphing UAV glider model is constructed, as shown in Fig. 4. The fuselage and wings are modeled separately with a 0.024 m clearance. The main parameters include a wingspan of 8.24 m, a wing area of 3.955 m^2, and a mean aerodynamic chord of 0.48 m. The wing uses a NACA4412 airfoil with a 2° incidence angle, while both the horizontal and vertical tails adopt a NACA0012 airfoil.



Folded Deployed

Figure 4 – LG2K-type folding morphing UAV glider model

The inertial parameters of the aircraft components are listed in Table (reference). The wing is connected to the fuselage via a revolute joint and rotates about the Z-axis of the body-fixed frame driven by a torsional spring. The deployment angle is defined as zero in the folded configuration with a locking angle of $\pi/2$. A torsional spring stiffness of 200 $\mathrm{N\,m\,rad^{-1}}$ is selected to ensure deployment within 0.5–0.6 s while accounting for aerodynamic damping effects.

Table 1 – Inertial properties of fuselage and wing

Parameter	Fuselage	Wing
Mass (kg)	360.0	20.0
Center of mass (m)	(1.201, 0, 0)	(3.24, -0.088, 0.38)
I_{xx} (kg·m^2)	20.21	0.38
I_{yy} (kg·m^2)	649.66	24.07
I_{zz} (kg·m^2)	653.44	24.45

2.4 Asymmetric Wing Deployment during Airborne Release

Flight tests have shown that folding morphing UAVs may exhibit asymmetric wing deployment during airborne release [17], as illustrated in Fig. 5, where the deployment angle difference between the left and right wings is approximately 20°. Although the configuration is geometrically symmetric, carrier wake effects may introduce sideslip relative to the incoming flow, resulting in asymmetric aerodynamic loads on the wings. Meanwhile, inertial coupling between vehicle attitude motion and wing deployment further influences the deployment dynamics. Under the combined effects of aerodynamic and inertial forces, asymmetric deployment and attitude response may occur, potentially leading to unstable flight trajectories or even collision with the carrier aircraft [18]. Therefore, further numerical investigation of the asymmetric deployment phenomenon and its influence on attitude evolution is necessary.

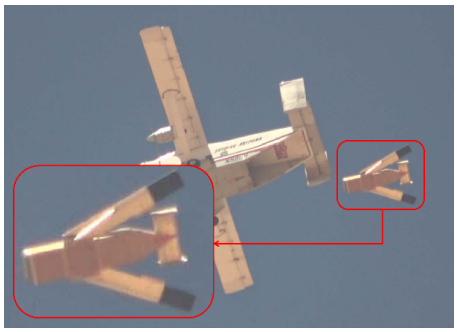


Figure 5 – Asymmetric deployment phenomenon during airborne release of the LG2K UAV

3. Results

3.1 Simulation Conditions and Computational Setup

Numerical simulations of the airborne deployment process are conducted under carrier wake effects represented by a sideslip angle. The freestream conditions are set to an angle of attack of 4°, a sideslip angle of 4°, a Mach number of 0.28, and an altitude of 2 km.

Two initial pitch-rate cases, corresponding to nose-up and nose-down conditions, are considered: $\omega_y = 1$ rad/s and $\omega_y = -1$ rad/s. The simulations are performed using Cartesian structured grids with approximately 1.337×10^6 cells. A fixed time step of 2.5 ms is adopted, and the total simulation time is 1.25 s.

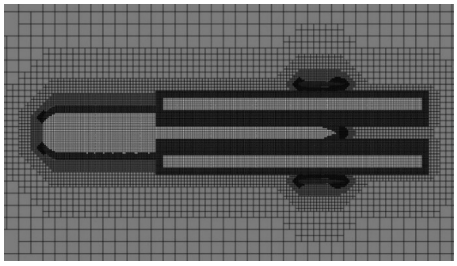


Figure 6 – Top view of computational grids around the aircraft at the initial state

3.2 Simulation Results and Attitude Evolution Analysis

Fig. 7 and Fig. 8 present the time histories of airborne deployment under two initial pitch-rate conditions. After release, the vehicle enters the wing deployment process accompanied by attitude variation, indicating significant aerodynamic–dynamic coupling characteristics. Under the combined effects of carrier wake disturbance and attitude motion, asymmetric wing deployment is observed during the deployment process.

Comparison of the two cases shows that the attitude evolution differs under different initial pitch rates. For the $\omega_y = 1\ \mathrm{rad/s}$ case, larger roll and attitude deflections are observed, whereas the $\omega_y = -1\ \mathrm{rad/s}$ case exhibits relatively weaker attitude evolution. The results indicate that the initial pitch rate has a significant influence on both attitude response and wing deployment behavior during airborne deployment.

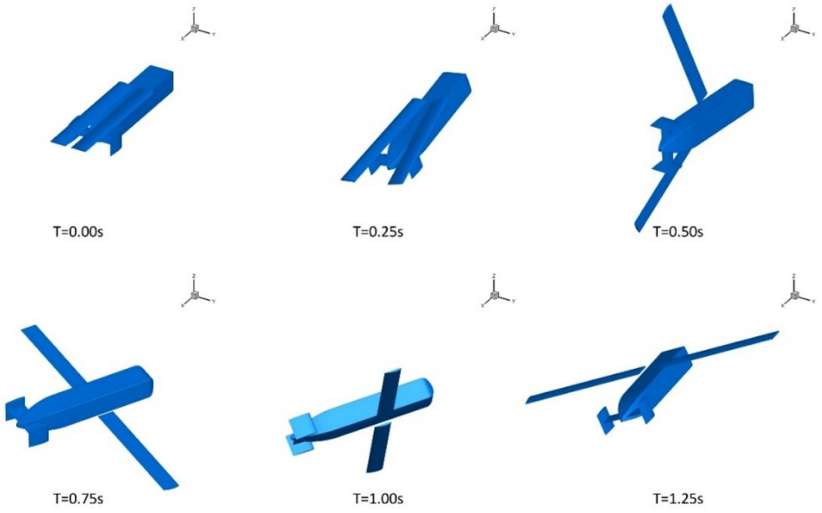


Figure 7 – Time history of airborne deployment with initial angular velocity $\omega_y = 1\ \mathrm{rad/s}$

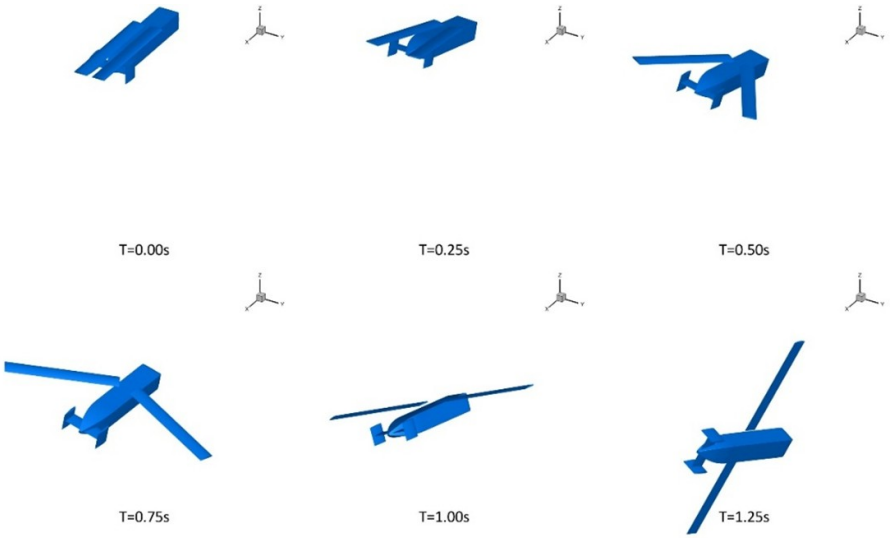
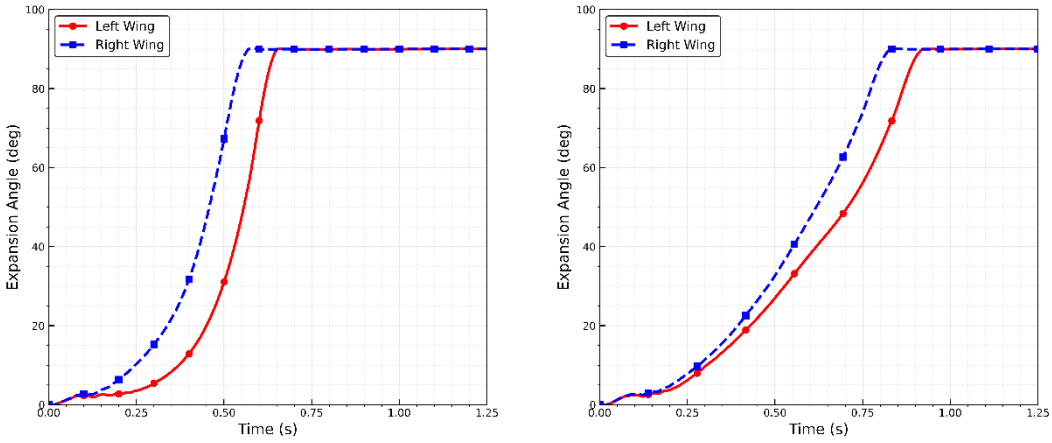


Figure 8 – Time history of airborne deployment with initial angular velocity $\omega_y = -1\ \mathrm{rad/s}$

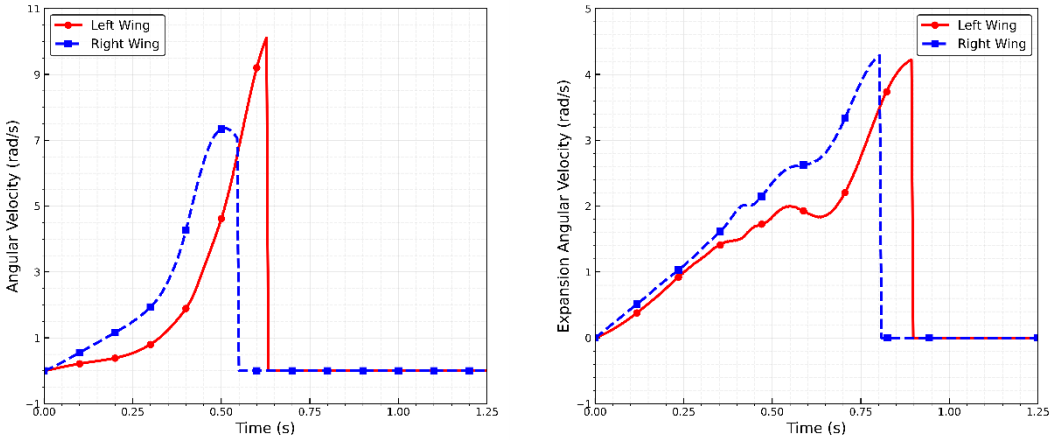
Fig. 9 and Fig. 10 show the time histories of wing deployment angles and deployment rates under the two initial pitch-rate conditions. Asymmetric wing deployment is observed in both cases, mainly reflected in differences in deployment rate and locking time. For the $\omega_y = 1\ \mathrm{rad/s}$ case, the right wing completes deployment at approximately 0.55 s, while the left wing locks at about 0.65 s, with a maximum deployment angle difference of approximately 35°. In contrast, the $\omega_y = -1\ \mathrm{rad/s}$ case exhibits relatively synchronized deployment, with the right and left wings completing deployment at

approximately 0.82 s and 0.9 s, respectively, and a maximum deployment angle difference of about 15°.



(a) Case of $\omega_y = 1$ rad/s (b) Case of $\omega_y = -1$ rad/s

Figure 9 – Time histories of left and right wing deployment angles



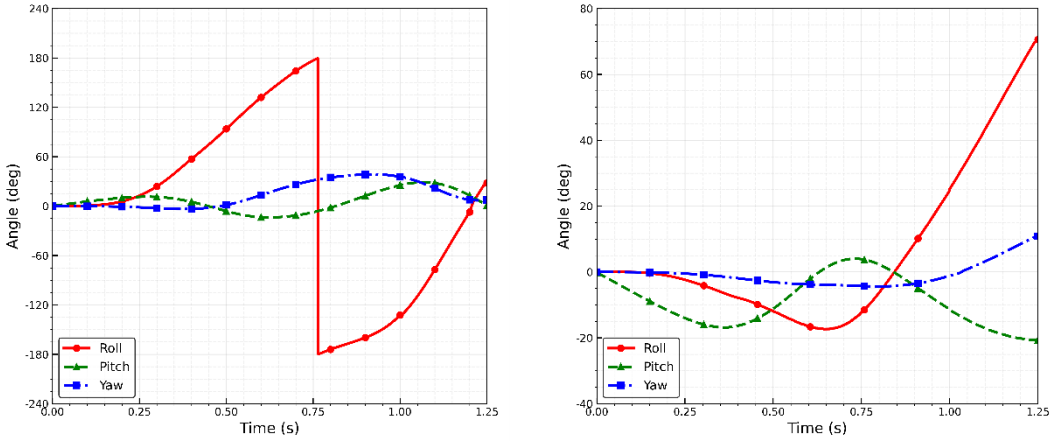
(a) Case of $\omega_y = 1$ rad/s (b) Case of $\omega_y = -1$ rad/s

Figure 10 – Time histories of left and right wing deployment rates

Asymmetric wing deployment further affects vehicle attitude evolution. Fig. 11 and Fig. 12 show the time histories of attitude angles and angular velocities under the two initial pitch-rate conditions. For the $\omega_y = 1$ rad/s case, earlier deployment of the right wing induces significant roll motion, with the roll angle exceeding 180° at approximately 0.75 s. In contrast, the $\omega_y = -1$ rad/s case exhibits more synchronized deployment and a weaker roll response, with a final roll angle of about 70° and a roll angular velocity of approximately 3 rad/s. The results indicate a strong correlation between wing deployment asymmetry and roll response intensity.

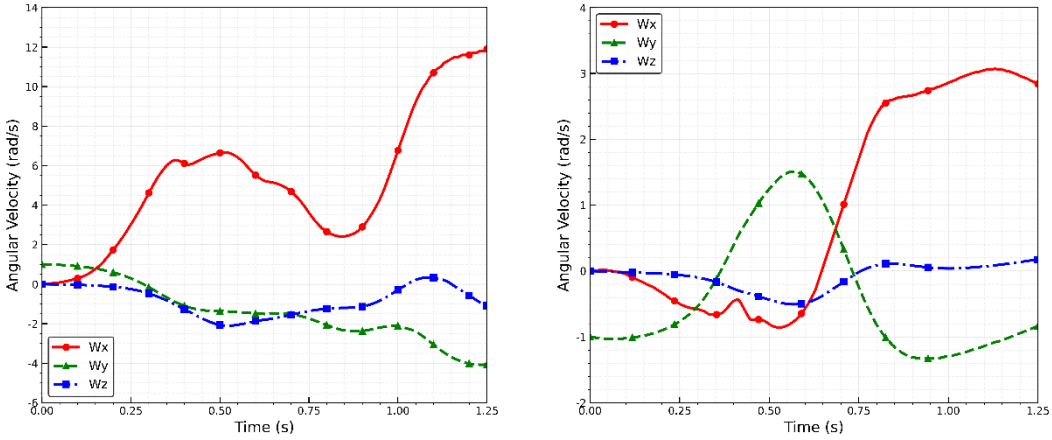
Fig. 13 and Fig. 14 show the time histories of centroid position and velocity under the two initial pitch-rate conditions. For the $\omega_y = 1$ rad/s case, the vehicle exhibits noticeable forward and upward motion during the later deployment process. In contrast, the $\omega_y = -1$ rad/s case remains in a descending state with negative V_z throughout the simulation. The difference in lateral displacement between the two cases is relatively small.

Fig. 15 shows the time histories of aerodynamic force components in the inertial frame, where F_x, F_y, and F_z denote the aerodynamic forces along the three coordinate directions. During the wing deployment process, all aerodynamic force components exhibit noticeable fluctuations, indicating strong unsteady aerodynamic effects that further influence vehicle attitude response and center-of-mass motion evolution.



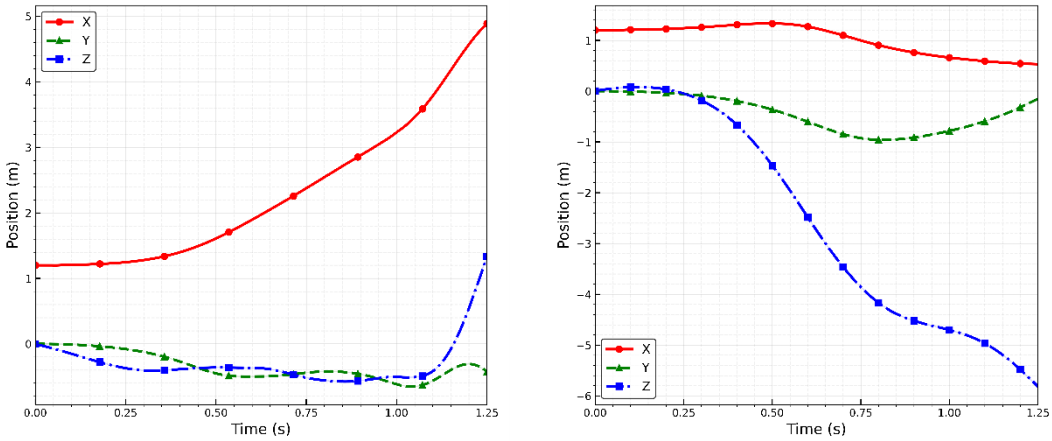
(a) Case of $\omega_y = 1$ rad/s (b) Case of $\omega_y = -1$ rad/s

Figure 11 – Time histories of aircraft attitude angles



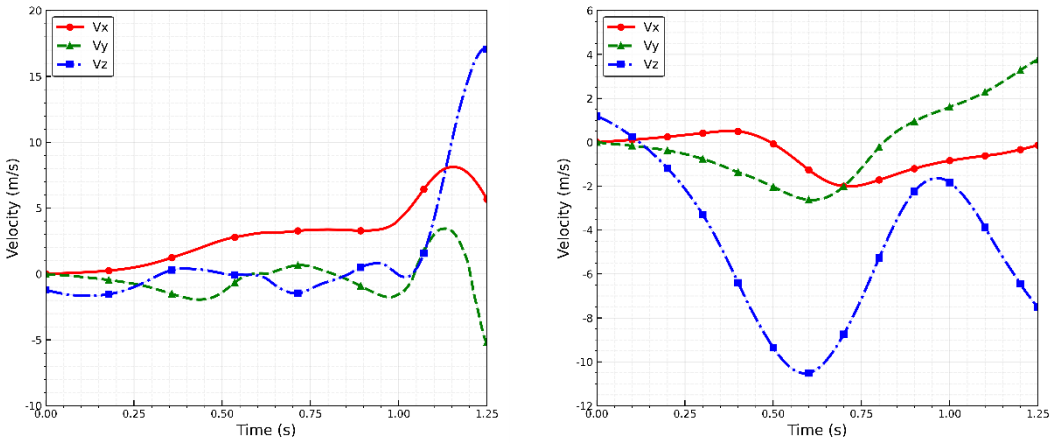
(a) Case of $\omega_y = 1$ rad/s (b) Case of $\omega_y = -1$ rad/s

Figure 12 – Time histories of aircraft angular velocities



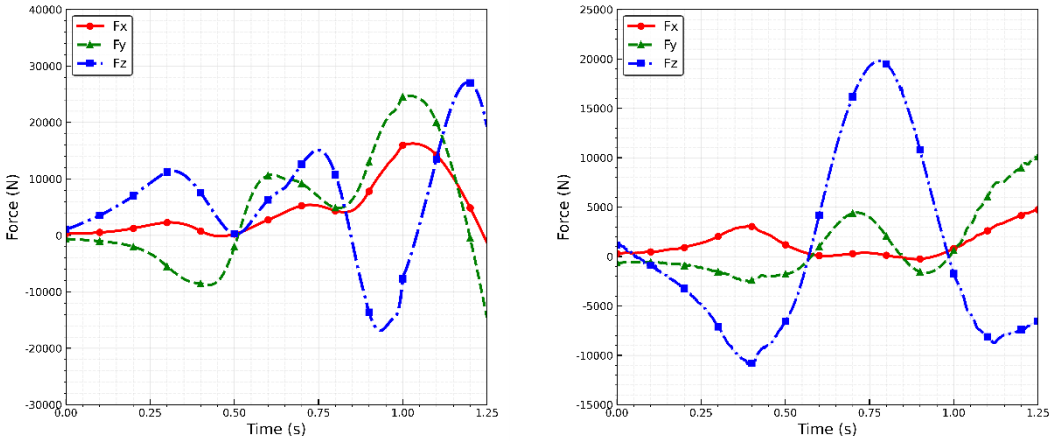
(a) Case of $\omega_y = 1$ rad/s (b) Case of $\omega_y = -1$ rad/s

Figure 13 – Time histories of aircraft centroid coordinates



(a) Case of $\omega_y = 1$ rad/s (b) Case of $\omega_y = -1$ rad/s

Figure 14 – Time histories of aircraft centroid velocities



(a) Case of $\omega_y = 1$ rad/s (b) Case of $\omega_y = -1$ rad/s

Figure 15 – Time histories of aircraft aerodynamic forces

The above results indicate that different initial pitch-rate conditions significantly affect wing deployment synchronization and the overall dynamic response of the vehicle. In the nose-up case, more pronounced asymmetric wing deployment is observed, accompanied by stronger roll response and larger spatial deviation. Meanwhile, the vehicle centroid exhibits an upward motion tendency during deployment, implying a potential collision risk with the carrier aircraft. In contrast, the nose-down case shows more synchronized wing deployment and smoother attitude evolution. Overall, a clear coupling relationship exists between asymmetric wing deployment and vehicle attitude motion during airborne deployment, which further affects center-of-mass motion characteristics through aerodynamic moments. The results demonstrate that the initial attitude motion state has an important influence on the deployment safety and attitude stability of folding morphing UAVs during airborne release.

4. Conclusion

This study investigates the large relative motion and strong aerodynamic interference during the airborne deployment of folding morphing UAVs using the developed aerodynamic–multibody dynamic coupling method. Numerical simulations are conducted to achieve a unified description of the dynamic behavior from airborne release to configuration deployment. Based on an LG2K-type folding morphing UAV configuration, comparative analyses are performed under different initial pitch-rate conditions while considering carrier wake effects. The results show that asymmetric wing deployment generally occurs during the deployment process, and different initial pitch states lead to distinct dynamic response characteristics. Under an initial nose-up pitch-rate condition, stronger deploy-

ment asymmetry is observed, accompanied by more significant attitude evolution and roll response, whereas the responses remain relatively moderate under an initial nose-down pitch-rate condition. The proposed coupling framework can effectively capture the major dynamic characteristics during airborne deployment and provides a useful reference for deployment analysis and scheme design of folding morphing UAVs. It should be noted that the present quasi-steady aerodynamic model still has limitations in capturing strong transient flow and local separation effects. Future work will further extend the simulation conditions and investigate additional initial conditions and flight states to improve the applicability of the method in complex airborne deployment environments.

5. Contact Author Email Address

Lei Qiao: ql@nwpu.edu.cn

6. Copyright Statement

The authors confirm that they, and/or their company or organization, hold copyright on all of the original material included in this paper. The authors also confirm that they have obtained permission, from the copyright holder of any third party material included in this paper, to publish it as part of their paper. The authors confirm that they give permission, or have obtained permission from the copyright holder of this paper, for the publication and distribution of this paper as part of the ICAS proceedings or as individual off-prints from the proceedings.

References

[1] Khasyofi M. The role of flight test data analysis in development flight testing. *International Journal of Aviation Science and Engineering-AVIA*, 5(2), 2023.

[2] Ratliff C. Marquart E. An assessment of a potential test technique-virtual flight testing (vft). In *Flight Simulation Technologies Conference*, p. 3415, 1995.

[3] Manning E. II T. Ratliff C. Marquart E. Bridging the gap between ground and flight tests-virtual flight testing (vft). In *Aircraft Engineering, Technology, and Operations Congress*, p. 3875, 1995.

[4] Ma Z. Smeur E J J. de Croon G C H E. Wind tunnel tests of a wing at all angles of attack. *International Journal of Micro Air Vehicles*, 14, 2022: 17568293221110931.

[5] Tang D. Dowell E H. Experimental aeroelastic models design and wind tunnel testing for correlation with new theory. *Aerospace*, 3(2):12, 2016.

[6] Jia S. Zhang Z. Zhang H. et al. Wind tunnel tests of 3d-printed variable camber morphing wing. *Aerospace*, 9(11):699, 2022.

[7] Bergmann A. Huebner A. Loeser T. Experimental and numerical research on the aerodynamics of unsteady moving aircraft. *Progress in Aerospace Sciences*, 44(2):121–137, 2008.

[8] Oberkampf W L. Trucano T G. Verification and validation in computational fluid dynamics. *Progress in Aerospace Sciences*, 38(3):209–272, 2002.

[9] Computational Fluid Dynamics Committee. Guide: Guide for the Verification and Validation of Computational Fluid Dynamics Simulations (AIAA G-077-1998 (2002))[J]. 1998.

[10] Pausch R. Crea T. Conway M. A literature survey for virtual environments: military flight simulator visual systems and simulator sickness. *Presence: Teleoperators & Virtual Environments*, 1(3):344–363, 1992.

[11] Yue T. Wang L. Ai J. Longitudinal linear parameter varying modeling and simulation of morphing aircraft. *Journal of Aircraft*, 50(6):1673–1681, 2013.

[12] Yue T. Wang L. Ai J. Multibody dynamic modeling and simulation of a tailless folding wing morphing aircraft. In *AIAA Atmospheric Flight Mechanics Conference*, p. 6155, Grapevine, 2009.

[13] Tong L. Ji H. Multi-body dynamic modelling and flight control for an asymmetric variable sweep morphing UAV. *The Aeronautical Journal*, 118(1204):683–706, 2014.

[14] Tong L. Ji H. Multi-body dynamic modelling and roll control of asymmetric variable sweep morphing aircrafts. In *2013 10th IEEE International Conference on Control and Automation (ICCA)*, pp. 1567–1572, IEEE, Hangzhou, 2013.

[15] Shi R. Wan W. Analysis of flight dynamics for large-scale morphing aircraft. *Aircraft Engineering and Aerospace Technology: An International Journal*, 87(1):38–44, 2015.

[16] An J. Yan M. Zhou W. et al. Aircraft dynamic response to variable wing sweep geometry. *Journal of Aircraft*, 25(3):216–221, 1988.

[17] Sarigul-Klijn M M. Sarigul-Klijn N. Gionfriddo M. Technology demonstration of a 1-ton single use disposable glider. In *AIAA Scitech 2019 Forum*, p. 2100, 2019.

[18] Feng H. A CFD/MBD Coupled Flight Simulation Methodology for Deployable Morphing Unmanned Aerial Vehicles. *Masters thesis*, Northwestern Polytechnical University, 2026.